Mixing and decomposition thermodynamics of c-Ti$_{1-x}$Al$_x$N from first-principles calculations

B. Alling,[1,2,][*] A. V. Ruban,[3] A. Karimi,[1] O. E. Peil,[4] S. I. Simak,[2] L. Hultman,[2] and I. A. Abrikosov[2]

[1]*Institute of Physics of Complex Matter, Swiss Federal Institute of Technology Lausanne (EPFL), 1015 Lausanne, Switzerland*
[2]*Department of Physics, Chemistry and Biology (IFM), Linköping University, SE-581 83 Linköping, Sweden*
[3]*Department of Material Science & Engineering, Royal Institute of Technology, Stockholm, SE-100 44 Sweden*
[4]*Condensed Matter Theory Group, Department of Physics, Uppsala University, SE-751 21 Uppsala, Sweden*

We describe an efficient first-principles method that can be used to calculate mixing enthalpies of transition metal nitrides with $B1$ structure and substitutional disorder at the metal sublattice. The technique is based on the density functional theory. The independent sublattice model is suggested for the treatment of disorder-induced local lattice relaxation effects. It supplements the description of the substitutional disorder within the coherent potential approximation. We demonstrate the excellent accuracy of the method by comparison with calculations performed by means of the projector augmented wave method on supercells constructed as special quasirandom structures. At the same time, the efficiency of the technique allows for total energy calculations on a very fine mesh of concentrations which enables a reliable calculation of the second concentration derivative of the alloy total energy. This is a first step towards first-principles predictions of concentrations and temperature intervals where the alloy decomposition proceeds via the spinodal mechanism. We thus calculate electronic structure, lattice parameter, and mixing enthalpies of the quasibinary alloy c-Ti$_{1-x}$Al$_x$N. The lattice parameter follows Vegard's law at low fractions of AlN but deviates increasingly with increasing Al content. We show that the asymmetry of the mixing enthalpy and its second concentration derivative is associated with substantial variations of the electronic structure with alloy composition. The phase diagram is constructed within the mean-field approximation.

I. INTRODUCTION

Transition-metal-nitride-based hard wear-resistant thin films have been commercially available for many decades. Alloying of TiN with Al was suggested in order to make the coatings more resistant against oxidation and the ternary nitride Ti$_{1-x}$Al$_x$N has become very popular in industrial applications. Several other transition metal nitrides have also been experimentally and theoretically investigated.[1–4]

Synthesized by vapor deposition techniques thin films of Ti$_{1-x}$Al$_x$N for $x < 0.7$ take the form of a cubic $B1$ (NaCl) structure substitutional disordered alloy where one of the two sublattices are occupied by randomly distributed Ti and Al atoms while the other sublattice is occupied by N atoms. However, the system is not stable and given that the amount of Al is large enough or that sufficient amount of thermal energy is supplied to the system a decomposition into wurtzite AlN and cubic TiN or Ti enriched Ti$_{1-x}$Al$_x$N takes place.

The efforts to develop Ti$_{1-x}$Al$_x$N has mainly been focused on methods, which, on the one hand, increase the Al content to promote oxidation resistance, while, on the other hand, prevent phase separation.[5] More recently it has been suggested that a spinodal decomposition of this pseudobinary nitride system might play an important positive role in the age hardening of the coating.[5] It has been shown to take place by the formation of coherent Ti-enriched Ti$_{1-x}$Al$_x$N regions and cubic AlN nanograins.[5,6]

Although significant understanding of the growth processes of transition metal nitrides have been achieved through *ab initio* calculations[7] and attempts have been made to simulate the effects of alloying on general phase stabilities in the Ti$_{1-x}$Al$_x$N system,[8] as well as in nitride based

semiconductors,[9–12] the nature of the decomposition in multicomponent nitride systems is not fully understood. An attempt made in Ref. 13 is subject to debate, as will be shown below.

In order to study the spinodal decomposition, the second concentration derivative of the mixing enthalpy needs to be calculated. This requires total energy calculations with small concentration intervals. This requirement is very computationally demanding within the conventional supercell technique. It would also be very difficult to eliminate numerical noise due to the quasirandom distribution of atoms in the supercells. On the other hand, the coherent potential approximation (CPA) based methods have proven very successful in *ab initio* total energy calculations of random alloys (see, for instance, Refs. 14 and 15). However, due to the use of a fixed ideal lattice geometry of the underlying crystal lattice, these methods cannot account directly for local lattice relaxation effects caused by a size mismatch of alloy components. Additional methods should therefore be used to treat these effects. In the case of relatively simple underlying lattices, such as face-centered cubic (fcc) or hexagonal closed packed (hcp), one can use, for instance, the effective tetrahedron model (ETM),[16,17] but if the lattice has more complicated structure, such as in $B1$ structure nitrides, a different structure specific consideration is needed. In this paper we introduce a model for the treatment of local lattice relaxations in $B1$ based compounds and apply it to Ti$_{1-x}$Al$_x$N alloys.

This paper is organized in the following way: In Sec. II theory and computational information about our calculations are given and our method for treating local relaxations is explained in detail. In Sec. III our results for the Ti$_{1-x}$Al$_x$N system regarding structural considerations, lattice parameters, electronic structure and thermodynamical properties
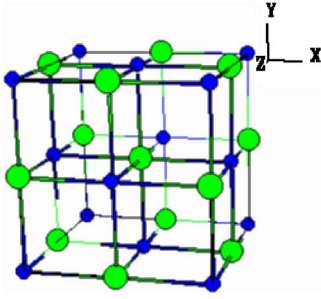
FIG. 1. (Color online) The *B*1 structure of TiN (Ref. 48) The structure consists of two fcc sublattices with the offsets (0,0,0) and (0.5,0,0). One of the sublattices is occupied by metal atoms while the other is occupied by nitrogen atoms.

are presented and discussed. In Sec. IV conclusions are drawn.

II. THEORY

A. Phase stability and spinodal decomposition

The thermodynamic stability of a solid solution as a function of alloy concentration x and temperature T can be described by its free energy $G(x,T)$. From a free energy vs composition diagram one can, by a common tangent construction, obtain the region(s) where the alloy is stable. However, immediately outside of this region the alloy can be metastable. The phase separation in this case can occur via nucleation and growth mechanism. A condition for this state is that the second concentration derivative of the free energy is positive. However, if instead

$$\frac{d^2G(x)}{dx^2} < 0, \tag{1}$$

the alloy is within the *spinodal region* and will decompose spontaneously through spinodal decomposition mechanism. In order to predict the spinodal regime it is therefore necessary to have a highly accurate description of the energy of the solid solution phase.

B. Exact muffin-tin orbitals method with nonequal sphere radii

The Green's function implementation[18–20] of the *exact muffin-tin orbitals* (EMTO) theory,[21–24] combined with the full charge density (FCD)[25,26] technique, has proved to be an efficient tool for accurate first-principles calculations of a wide spectrum of properties of different systems,[19,20,27–29] including random alloys.[15,30–34] One of the main advantages of the method is the use of optimized overlapping muffin-tin (OOMT) potentials constructed directly from the full potential. This provides an accurate representation of the one-electron potential. As an output from EMTO calculations one obtains the self-consistent Green's function and one-electron states, and, as a final result one reconstructs the complete nonspherical one-electron density. The total energy is calculated using the full charge density (FCD) method with the
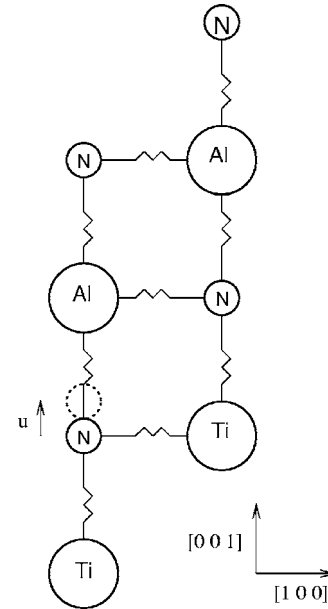
FIG. 2. The structure used to calculate the parameters of the independent sublattice model v_{ij}, Eqs. (5) and (6), in the case of c-Ti$_{1-x}$Al$_x$N. It is an ordered structure on the *B*1 underlying crystal lattice, in which the metal atoms in the [001] planes follow the ordered sequence Ti-Ti-Al-Al-Ti-Ti-Al-Al, etc. The (exaggerated) displacement of a nitrogen atom by vector **u** from its ideal *B*1 position is also shown.

shape function technique[36] utilized to integrate the density over a unit cell.

The integration technique makes the calculation somewhat dependent on the division of space into regions associated with particular atoms in the unit cell. For systems with atoms of similar sizes division into ordinary Wigner-Seitz cells (Voronoi diagram on a set of atomic positions) turns out to be appropriate. However, for systems with atoms of essentially different radii, as is the case for Ti$_{1-x}$Al$_x$N alloys, the sizes of the potential spheres must be properly adjusted to perform accurate optimization of the potential, and to avoid cutting off of the atomiclike wave functions by the unit cell boundaries. In the current implementation of the EMTO method space division is consistent with the radii of potential (MT) spheres, and if potential sphere are set to be of different sizes, then multiplicatively weighted Voronoi diagram is constructed instead of Wigner-Seitz cells.

The procedure of choosing the potential sphere radii ratio should, in principle, be included into the self-consistent scheme as a part of the fit of a full potential by a set of overlapping spherical ones. But in fact calculations show that bulk ground-state properties depend only slightly on the radii ratios in a certain range of the ratio values, and one can, therefore, fix the ratio in such a way that the results are insensitive to small variations of the potential sphere radii.

In the present calculation the ratio of the potential sphere radii for both Ti and Al with respect to N is taken to be 1.27:1 (which corresponds to 1.3:1 in terms of the ratio of the inscribed sphere radii and leads to a minimal value of the potential discontinuity at the potential sphere boundary), and it is fixed for the whole concentration range.
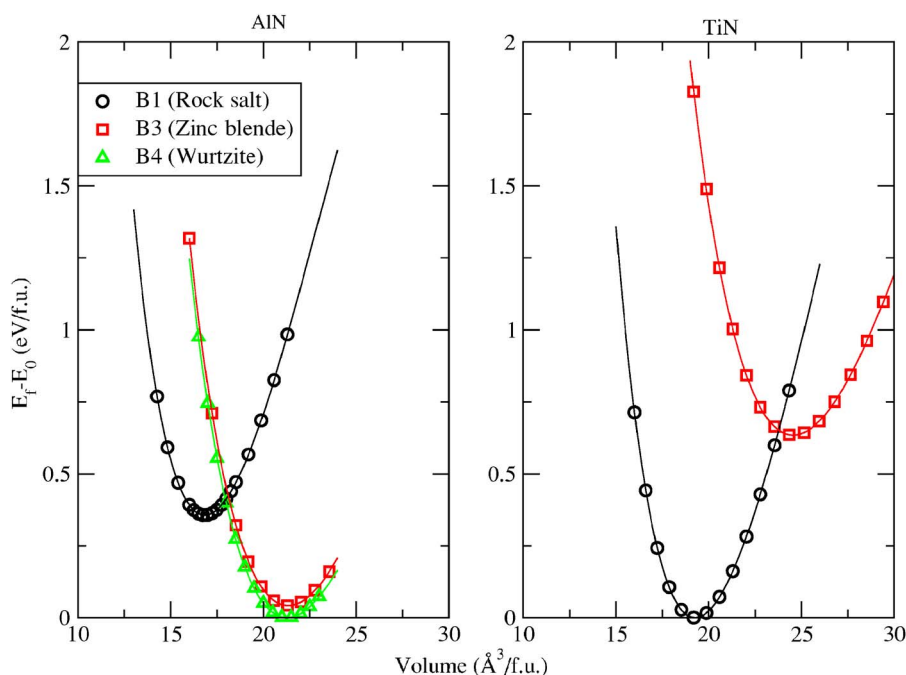
FIG. 3. (Color online) The equation of states for the $B1$ (NaCl), $B3$ (ZnS), and $B4$ (wurtzite) structures of AlN and for the $B1$ and hypothetical $B3$ of TiN as calculated using the PAW method.

We have used the CPA[30] to treat the substitutional disorder on the metal sublattice and the generalized gradient approximation, GGA,[37] have been used for the exchange-correlation energy. Using the order-N locally self-consistent Green's function method,[38,39] we have checked that the neglect of local environment effects in the CPA does not change our results for a random atomic distribution. An investigation of possible short-range order effects in this system is beyond the scope of the present work. We have calculated total energies for 21 concentrations uniformly distributed over the whole concentration interval of $Ti_{1-x}Al_xN$ alloys with steps of five percents.

C. Supercell calculations of random alloys

In order to check the accuracy of the CPA-based total energy calculations and to obtain information on the contribution to the alloy total energy due to local lattice relaxation, we carried out several supercell calculations for alloy compositions $x=0.125, 0.25, 0.375, 0.50, 0.625, 0.75$, and 0.875 as well as for pure TiN and cubic $B1$ AlN using the projector augmented wave (PAW) method[40] in the generalized gradient approximation[37] for the exchange-correlation energy as implemented in the VASP code.[41,42]

Actually the choice of a supercell, which models a random alloy, is not a trivial task. The problem is that whether a supercell can be considered as random or not in the total energy calculations is exclusively dictated by the nature of the effective interactions in the system.[39] This is so since the total energy of any alloy configuration (let us denote the latter by p) at a fixed alloy composition can be presented in terms of the effective interactions as

$$E_p = E_{rand} + \sum_f V_f(\alpha_p^f - \alpha_{rand}^f), \qquad (2)$$

where V_f are the so-called effective interactions for cluster f;[43] α_p^f denotes the corresponding correlation functions of the

p configuration of the alloy,[44,45] which in our case correspond to a particular distribution of atoms in the supercell, and α_{rand}^f are the correlation functions of a random alloy.

It is obvious from Eq. (2), that the only way to obtain the total energy of a random structure right using an ordered supercell is to satisfy two conditions: (1) $V_f=0$ for for all figures f, for which $\alpha_p^f \neq \alpha_{random}^f$ and vice versa and (2) $\alpha_p^f = \alpha_{random}^f$ for all f, for which $V_f \neq 0$. Since the effective interactions are usually quite long ranged, these conditions are never satisfied in the supercell calculations exactly.

In the case of the special quasirandom structures (SQS) originally proposed by Zunger et al.[46,47] for some fcc random alloys, the second condition is specified just for the first few coordination shells. In many cases such a supercell give a reasonable representation of a random alloy due to the fact
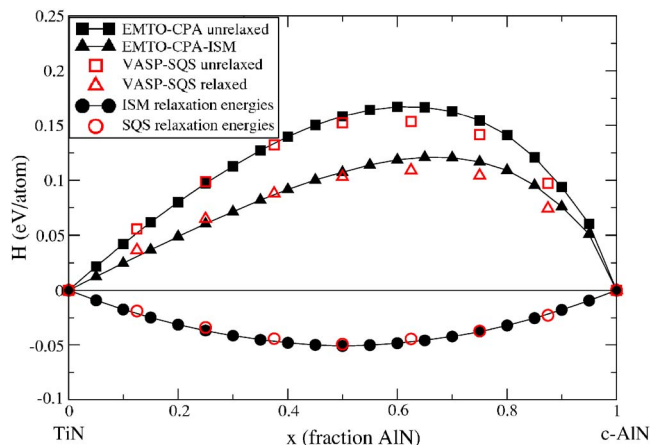
FIG. 4. (Color online) Mixing enthalpy, H, of c-$Ti_{1-x}Al_xN$ calculated with EMTO (solid symbols) and PAW (open symbols) methods. The unrelaxed values are shown with squares and the relaxed values with triangles. Also the relaxation energies are shown with circles.
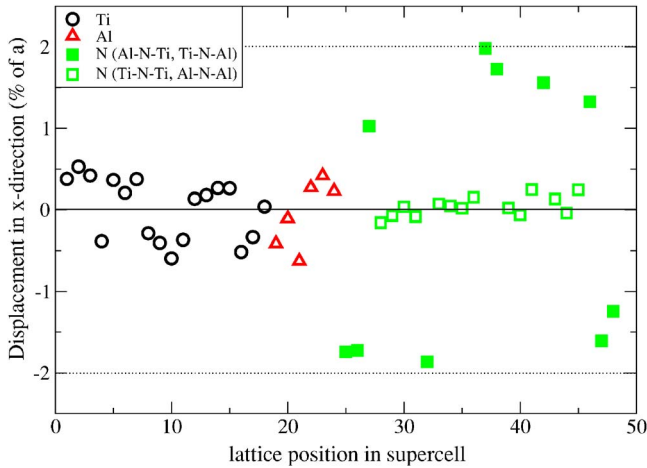
FIG. 5. (Color online) Relaxation pattern in the x direction for the atoms in the Ti$_{0.75}$Al$_{0.25}$N supercell. Ti atoms are marked with black circles (positions 1–18), Al atoms with red triangles (positions 19–24). N atoms surrounded by one Al and one Ti atom along the x direction are marked with solid green squares while N atoms surrounded by two chemically equivalent metal atoms are marked with open green squares (all N's, positions 25–48). The dotted lines show the relaxation of a N atom in the pseudo-$Z2$ ordered structure shown in Fig. 2. The latter was used to determine parameters of the ISM, Eqs. (5) and (6).

that the strongest effective interactions in alloys are usually at the nearest-neighbor coordination shells. It is clear, that the quality of a SQS is improving with the number of correlation functions satisfying the second condition. It is also obvious what total energies calculated with supercells, where the correlation functions are not controlled, e.g., with *ad hoc* constructed supercells, may lead to unpredictable results even if one carries out an averaging over several (but still limited) number of different supercells.

A more general recipe for choosing the best possible supercell for a given system is the following: One should find effective cluster interactions in the system and then construct a supercell in which α_p^f are as close as possible to α_{rand}^f for those clusters f, for which V_f is not negligible. Such a recipe is a natural extension of the original SQS method,[46,47] but brings the focus to assessing convergence of Eq. (2).

We have checked the effective pair interactions on the Ti-Al subblatice in (Ti, Al)N by using the screened generalized perturbation method (SGPM),[35] and found that the strongest effective cluster interactions are the pair interactions on the first five coordination shells (also there are significant three-site and four-site interactions). Therefore, we have constructed supercells, whose Warren-Cowley short-range order parameters are almost exactly equal to those in a completely random alloy, with deviations not greater than 5%, at the first five coordination shells of the Ti-Al sublattice. Also for the sixth and seventh Ti-Al coordination shells the short-range order parameter is close to those in a completely random alloy, with deviations smaller than 15%. For $x=0.25$, 0.5, and 0.75, we have used 48-atom [24-(Ti, Al) and 24-N] supercells and for $x=0.125$, 0.375, 0.625, and 0.875—64-atom [32-(Ti, Al) and 32-N] supercells. The distributions of atoms in the supercells are given in the Appen-
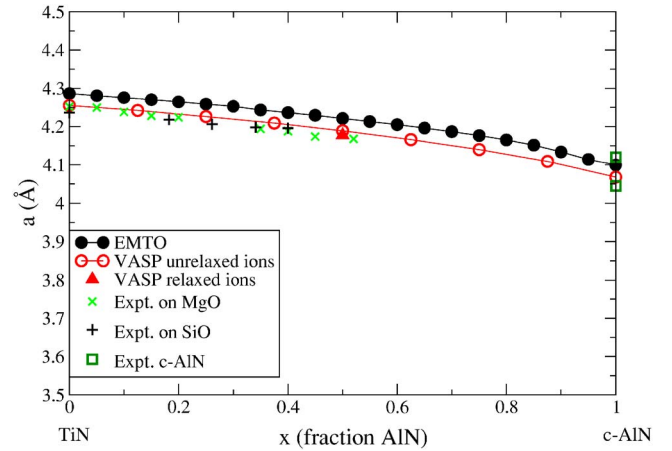
FIG. 6. (Color online) The lattice parameter a of Ti$_{1-x}$Al$_x$N as a function of the fraction of AlN, x. The values obtained from both EMTO (filled circles) and PAW-supercell (unrelaxed ions: open circles, relaxed ions: filled triangle) methods are shown together with the results of two different epitaxial thin film experiments ("x" symbol, Ref. 48; "+" symbol, Ref. 50) and two different alloy experiments (open squares, Refs. 51 and 52) for cubic AlN.

dix together with the corresponding short-range order parameters.

In our supercell simulations both ionic positions and volume have been relaxed. The calculations for the (Ti$_{50}$Al$_{50}$)N alloy show that the differences in the total energy and equilibrium lattice spacing are minimal between the results obtained by relaxing the ionic positions for all volumes and the results obtained when the ionic relaxation are carried out only for the equilibrium volume, which is calculated for the ideal $B1$ structure. For the other concentrations the latter approach have been used.

D. Independent sublattice model for local lattice relaxations

In Fig. 1 we show the $B1$ structure considered in this work.[48] This structure consists of two interpenetrating fcc sublattices. The first sublattice with the offset (0,0,0) is for transition metal nitrides occupied by metal atoms while the second sublattice with the offset (0.5,0,0) is occupied by nitrogen atoms. In the ground state of pure TiN as well as in the cubic $B1$ phase of AlN the atoms occupy these ideal lattice positions and all nearest-neighbor bonds are of equal length. However, due to the difference in lattice parameter between TiN and c-AlN this will no longer be the case in a random substitutional Ti$_{1-x}$Al$_x$N alloy. Although the absolute shift of ions off their ideal $B1$ positions might be small, the energy that the system gains by relaxing all individual ionic position can be large due to the strong bonds between metal and nitrogen nearest neighbors in transition metal nitrides. The relaxation energy is defined as

$$E_{rel}(x_1, x_2, \dots) = E_{tot}(x_1, x_2, \dots) - E_{unrel}(x_1, x_2, \dots) \quad (3)$$

where $E_{tot}(x_1, x_2, \dots)$ is the total energy for a system with the concentrations x_1, x_2, etc. of the different alloy components and with fully relaxed ionic positions while $E_{unrel}(x_1, x_2, \dots)$
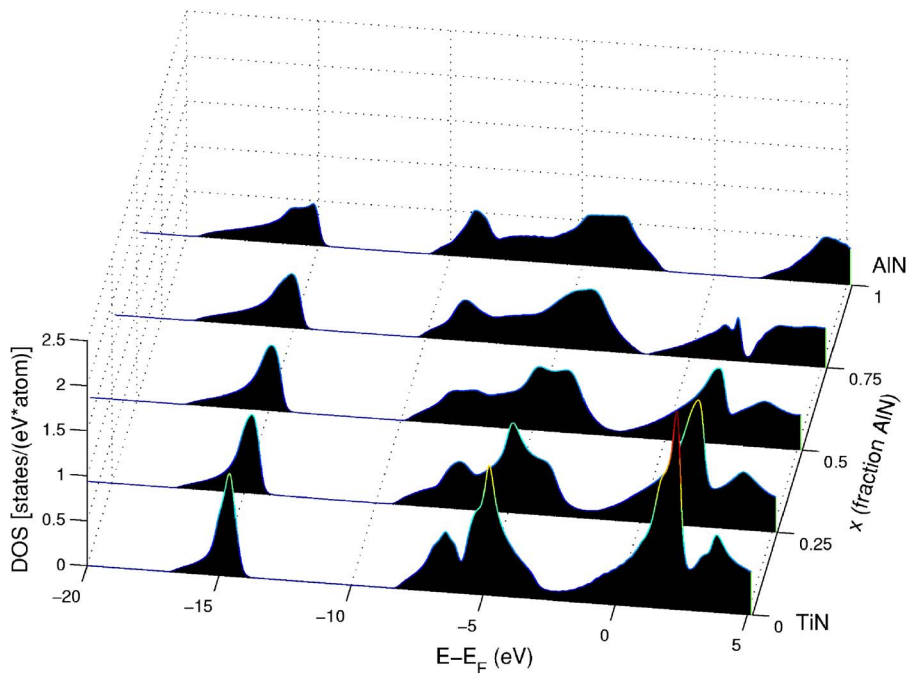
FIG. 7. (Color online) Total density of states (DOS) for c-$Ti_{1-x}Al_xN$ as calculated with the EMTO-CPA method. The DOS are shown for different fractions x of AlN: 0.00, 0.25, 0.50, 0.75, and 1.00. Note the band gap present in the semiconductor c-AlN.

is the total energy calculated for the same system when all atoms are placed on ideal lattice positions.

The local lattice relaxations are straightforwardly taken into consideration in the supercell calculations. In the EMTO-CPA approach, on the other hand, this is not possible and therefore they should be treated separately. One method to do this, the effective tetrahedron method (ETM), is proven to work well in some metallic alloys with relatively simple crystal structures (fcc).[16] The ETM considers the effect of a local volume relaxation of small clusters of different composition in the alloy. In the $B1$-nitride case one needs, however, to consider the additional effect of the relaxation of the nitrogen and metal atoms relative to each other. For this purpose, we propose here the independent sublattice model (ISM).

In order to understand the mechanism behind the local relaxations in $Ti_{1-x}Al_xN$ we note that it is only one of the two sublattices, the metal sublattice, that shows a random distribution of atoms. This is true since we in this work neglect nitrogen vacancies and consider N sublattice as completely homogeneous. The treatise of nitrogen vacancies is the topic of an ongoing study. This means that the metal atoms all have chemically equivalent nearest neighbor nitrogen atoms, while the later have different nearest-neighbor environments. For this reason, N is more likely to show considerable displacement from their ideal $B1$ positions than the metal atoms. We therefore divide the relaxation energy into two parts, corresponding to independent relaxations of the two sublattices in the $B1$ structure:

$$E_{rel}^{ISM}(x_1, x_2, \ldots) = E_{N\ rel}(x_1, x_2, \ldots) + E_{metal\ rel}(x_1, x_2, \ldots),$$

$$(4)$$

where $E_{N\ rel}(x_1, x_2, \ldots)$ is the energy gained by relaxing the positions of the nitrogen atoms in the alloy with concentration x_1 of the first metal component, x_2 of the second, etc.,

assuming that the metal atoms occupy ideal fcc lattice positions. The second term, $E_{metal\ rel}(x_1, x_2, \ldots)$, is the energy that the system gains by relaxing the positions of the metal atoms, which can be calculated following the ETM scheme.[16]

Let us consider the first term of the right-hand side of Eq. (4). The nitrogen atoms occupy octahedral positions and have two metal atoms in opposite directions along the x, y, and z axes (see Fig. 1). If one assumes that the relaxation of N atoms are only effected by their nearest neighbors one can show by spring model arguments that in a random alloy

$$E_{N\ rel}(x_1, x_2, \ldots) = 3 \sum_{i=M_1,M_2,\ldots} \sum_{j=M_1,M_2,\ldots} v_{ij} p_{ij}(x_i, x_j). \quad (5)$$

The factor 3 comes from the three dimensions in which the atom can move. The sums are taken over the different me-
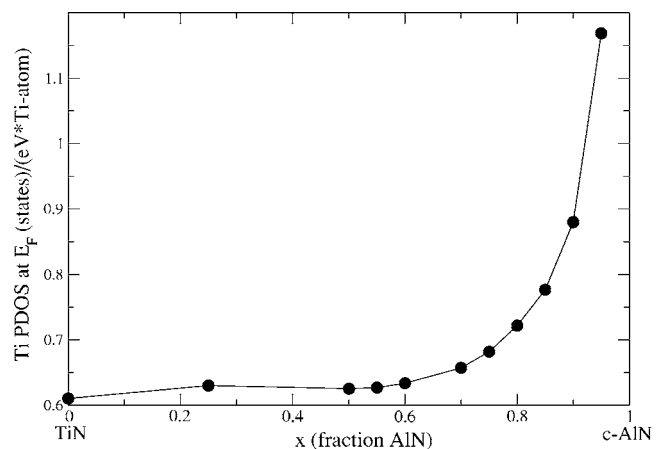
FIG. 8. Ti-site projected density of states (pDOS) at E_F in units of states/(eV*Ti-atom) as a function of fraction of AlN x calculated with the EMTO method.
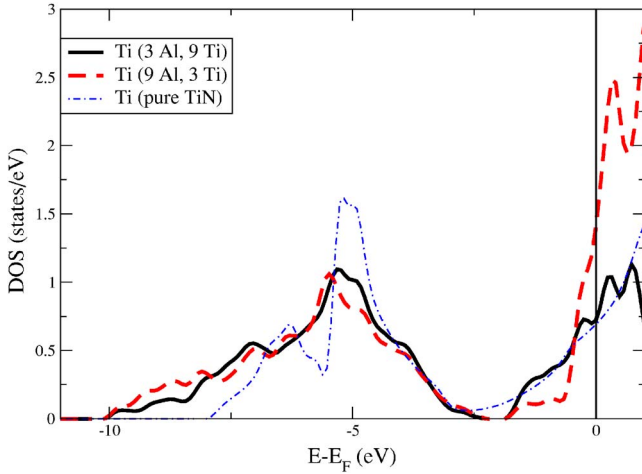
FIG. 9. (Color online) The site projected DOS at Ti atoms in different local environments within c-Ti$_{0.5}$Al$_{0.5}$N in states/eV as calculated for supercells by PAW. The local DOS of one Ti atom with 3 Al and 9 Ti next-nearest neighbors (solid line) and one Ti atom with 9 Al and 3 Ti next-nearest neighbors (dashed line) are shown together with the Ti-site projected DOS in pure TiN (dash-dotted line).

tallic alloy components (denoted as M_1, M_2 above), which can occupy the two metal-sites neighboring N in each direction, so that all possible metal-N-metal triplets present in the alloy are included in the summation. In Eq. (5) v_{ij} is the relaxation energy gained by shifting an N atom positioned between one metal atom of sort i and one of sort j, while $p_{ij}(x_i,x_j)$ denotes the probability that the neighboring metal on one side of the nitrogen atom is of sort i and the metal on the opposing side is of sort j. Due to the symmetry of the $B1$ crystal lattice $v_{ii}=0$ and $v_{ij}=v_{ji}$ in the nearest-neighbor approximation. Of course $p_{ij}(x_i,x_j)=p_{ji}(x_i,x_j)$. In the case of a ternary alloy with two metal components such as Ti$_{1-x}$Al$_x$N, Eq. (5) is simplified to

$$E_{N\ rel}(x) = 6v_{12}x(1-x). \tag{6}$$

The energies v_{ij} can be calculated by considering relaxation energies in an *ordered* structure on the underlying $B1$ crystal lattice. In this work we used the structure shown in Fig. 2. In this structure metal atoms occupy positions corresponding to a "double $L1_0$," also called $Z2$, structure. This is the smallest ordered structure within a fcc framework that allows us to estimate v_{12} in Eq. (6), because in this structure N atoms are indeed surrounded by metal atoms of different sorts along [001] direction. The relaxation energy can be calculated by the PAW method, as is done in this work, or with any method that allows for the geometry optimization. Of course the method used for the geometry optimization should be consistent with the method in which the CPA is implemented. This is the case with EMTO and PAW as will be shown in the next section.

When $E_{N\ rel}(x_1,x_2,\dots)$ and $E_{metal\ rel}(x_1,x_2,\dots)$ have been calculated one can easily obtain the total relaxation energy by Eq. (4), and then calculate the total energy of the alloy as
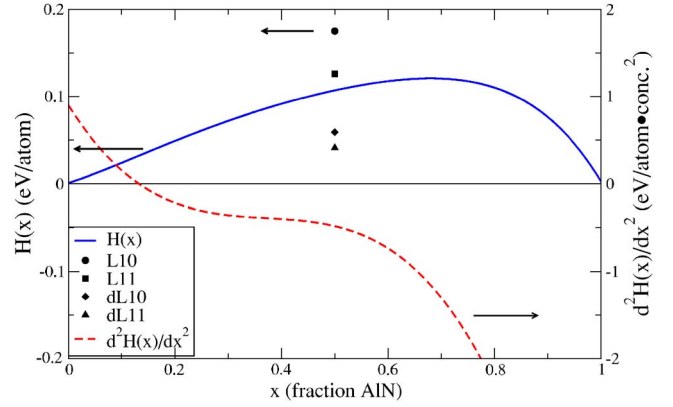
FIG. 10. (Color online) Mixing enthalpy of a random solid soulution of c-Ti$_{1-x}$Al$_x$N as a function of fraction of AlN together with its second concentration derivative. Also shown are the enthalpy values of four different ordered Ti$_{0.5}$Al$_{0.5}$N compounds. Se text for discussion.

$$E_{tot}(x_1,x_2,\dots) = E_{unrel}(x_1,x_2,\dots) + E_{rel}^{ISM}(x_1,x_2,\dots). \tag{7}$$

III. RESULTS

A. Structural considerations

TiN crystalizes in the rock salt, $B1$, structure while the ground state for AlN is wurtzite, $B4$. When synthesized by physical vapor deposition technics Ti$_{1-x}$Al$_x$N has the $B1$ structure for AlN fraction up to about $x=0.67$ and a mixture of $B1$ and $B4$ phases for higher AlN content.[5] In Fig. 3 the total energy of $B1$ (rock salt), $B3$ (zinc blende), and $B4$ (wurtzite) structures of AlN, and the $B1$ and (hypotetical) $B3$ phase of TiN is shown as a function of volume as calculated with the PAW method. The energy is given relative to the total energy of the ground state. The existence of a high-pressure cubic $B1$ phase of AlN is clearly visible. This structure is 0.36 eV/f.u. higher in energy but has a considerable lower volume than the ground-state wurtzite structure. The other cubic phase of AlN, zinc blende, is only slightly higher in energy (0.04 eV/f.u.) than the wurtzite phase but it has almost the same equilibrium volume as one can see in Fig. 3. There is no pressure-induced transition to this structure within the volume intervals considered in this work. For TiN the $B1$ ground state is far below the energy minima of both $B3$ (0.63 eV/f.u.) and $B4$ (4.52 eV/f.u. not shown in the figure) structures.

The existance of a metastable $B1$ phase of AlN with a relativly small volume missmatch to TiN together with the high energy of $B3$ and $B4$ phases of TiN and the large difference in volume to the $B4$ structure of AlN is the driving force that leads to the stabilization in the coherent $B1$ structure over a large concentration range in Ti$_{1-x}$Al$_x$N as seen in experiments. Of course, such $B1$ samples can only be metastable and if the AlN content is high enough or if the material is subject to very high temperatures, some AlN will overcome the nucleation barrier and transform into its ground state $B4$ structure with considerably larger volume. Such a transformation between phases cannot take place by spinodal
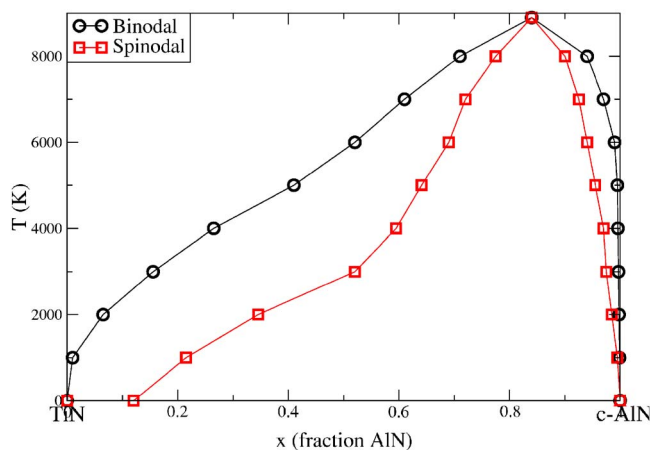
FIG. 11. (Color online) The mean-field estimate of the composition-temperature phase diagram of c-Ti$_{1-x}$Al$_x$N. The binodal is shown with circles and the spinodal with squares.

decomposition. However, within the $B1$ structure framework the isostructural decomposition can and does take place, as has been observed experimentally. This isostructural transition is the main subject of this work. No signs of zinc blende phases have been experimentally observed in Ti$_{1-x}$Al$_x$N which has been explained by the large volume barrier between the $B1$ and $B3$ phases.[6] In the remaining part of this paper we consider only $B1$ structure of the alloy and we use c-AlN as abriviation for $B1$ AlN since this is a generally accepted terminology for this material.

B. Mixing enthalpy and local relaxations in Ti$_{1-x}$Al$_x$N

Figure 4 shows the mixing enthalpy of c-Ti$_{1-x}$Al$_x$N calculated as

$$H(x) = E(c\text{-Ti}_{1-x}\text{Al}_x\text{N}) - (1-x)E(c\text{-TiN}) - xE(c\text{-AlN}),$$

$$(8)$$

with PAW using supercells and with the EMTO-CPA method, for both cases where the atoms are placed at ideal $B1$ lattice positions and when local relaxations are considered. The relaxation energies themselves are also shown.

One can clearly see in Fig. 4 that including local relaxations lowers the mixing enthalpies by up to one third. Thus, one cannot approximate substitutional disorder in this system by considering random occupation at sites of an ideal underlaying $B1$ lattice.

We calculate $v_{\text{TiAl}} = 0.030$ eV/atom in Eq. (5). For the alloy with $x = 0.5$, this gives $E_{N\ rel}(0.5) = 0.045$ eV/atom. Using the ETM for the local cluster volume relaxation energy of the metal sublattice we obtain $E_{metal\ rel}(0.5) = 0.005$ eV/atom which adds up to $E_{rel}^{ISM}(x) = 0.050$ eV/atom in excellent agreement with the supercell value for this concentration, 0.049 eV/atom. As can be seen in Fig. 4 the ISM model for local relaxations works extremely well for all concentrations where the supercell energies have been calculated.

In Fig. 5 we show the displacement of the atoms in the fully relaxed supercell, which models Ti$_{0.75}$Al$_{0.25}$N alloy. We show the values of the displacements projected in the x di-

rection. One can clearly see that N atoms that are surrounded along the x axis by two metallic atoms of different kinds (solid green squares in Fig. 5) show the largest displacements, 1–2 % of the average bond length. Note that the values are in agreement with the displacements of the N atom in the pseudo-$Z2$ ordered compound used for the determination of the parameters of the ISM (shown by the dotted lines in Fig. 5). At the same time, the N atoms that are surrounded along the x direction by two chemically equivalent atoms show negligible displacements (0.1–0.3 % of the average bond length). The metal atoms themselves show small displacements that are consistent with the small values of local cluster volume relaxations obtained within our ETM calculations. The same relaxation behavior is obtained in the supercells with different compositions.

From the considerations above, it is obvious that the approximations done in deriving the ISM model are justified and that the model itself captures the relevant physics behind the local relaxation phenomenon in this system very well. The relaxation energies for all concentrations are in excellent quantitative agreement with the supercell calculations and the actual relaxation patterns are qualitatively captured. We therefore expect this to be the case also in other metal nitrides with the $B1$ structure.

C. Concentration dependence of lattice parameter

In Fig. 6 the equilibrium lattice parameters of Ti$_{1-x}$Al$_x$N calculated both with the EMTO and with PAW methods are presented. Two different epitaxial experiments[49,50] are shown together with two different experimental results for the lattice parameter of $B1$-structured AlN synthesized in high-pressure experiments.[51,52] The lattice parameter of $B1$ AlN obtained in these experiments differ substantially from each other: 4.12 Å in Ref. 51 and 4.045 Å in Ref. 52. The experimental value for the lattice parameter of TiN is 4.24 Å.[51] Experimentally it has been shown that the lattice parameter of Ti$_{1-x}$Al$_x$N decreases linearly as a function of Al content.[49,50] For large x, it is very difficult to synthesize the alloy samples, due to a strong driving force for phase separation, and therefore the studies of lattice parameter are experimentally limited to x below about 0.7.

The calculated values of the lattice parameter are in good agreement with the experimental data. The values for pure TiN are 4.29 Å (EMTO) and 4.26 Å (PAW). This corresponds to an overestimation by about 1% and 0.3%, respectively. Such a small overestimation is common for GGA calculations. Our calculated values for pure c-AlN, 4.10 Å (EMTO) and 4.07 Å (PAW), are between the experimental values from Refs. 51 and 52. However, correcting our results for the overestimation of lattice parameter of the same magnitude as in TiN, the lower experimental value achieved in Ref. 52 seems trustworthy.

The lattice parameter furthermore exhibits an essentially linear dependence on AlN fraction x although a slight deviation is present above $x = 0.70$. However, this deviation from Vegard's law appears at high x, above the values at which experiments were performed.

When performing supercell calculations for alloys, we find that the difference between the equilibrium lattice pa-

rameters of the supercells with ideal $B1$ positions and fully relaxed positions is practically negligible. The equilibrium lattice parameter for the supercell with relaxed ionic positions is shown in Fig. 6 with a filled triangle. The supercell corresponds to the composition $x=0.50$ where relaxation effects should be largest.

Due to the relatively small difference in lattice parameters between TiN and c-AlN, 3–5 % depending on which experiment to trust, the large mixing enthalpy as shown in Fig. 4 is not likely to be more than to a small part due to volume mismatch. A comparison can be made with the electronically well-matched system $In_xAl_{1-x}N$.[10] In that system the difference in lattice parameters is much larger, about 12%, while the mixing enthalpy is only about half the value of the mixing enthalpy of $Ti_{1-x}Al_xN$.[10] Instead, in the next section, we search for an explanation based on the consideration of the electronic structure.

D. Density of states and binding character

It is well established that the bonding in TiN as well as in the related compound TiC has a mixed character of both covalent, ionic, and metallic bonds.[53–56] N $2p$-Ti$3d$ hybridization leads to formation of covalent bonding and antibonding states. However, the symmetry of the $B1$ structure only allows Ti $3d$ states with e_g symmetry to hybridize with the N $2p$ states while the d states with t_{2g} symmetry form so-called nonbonding states and account for weak hybridization between next-nearest- neighbor Ti atoms.[56] Even though the extent of overlap between Ti d states for the next-nearest-neighboring Ti atoms have been shown to be small for states below the Fermi level[53] this hybridization broadens the nonbonding state to form a shoulder at the density of states (DOS) curve[57] that in TiN is occupied. Due to the difference in electronegativities a large charge transfer occurs from Ti to N leading to an ionic admixture to the bonding.

In cubic AlN, on the other hand, the ionic bonds have been shown to dominate.[58] This is different to the case of wurtzite AlN where covalent bonding is also present.[58]

Due to the differences between TiN and c-AlN one can expect that the electronic structure effects will give strong variation of the properties of metastable $Ti_{1-x}Al_xN$ as a function of composition. In Fig. 7 we show the calculated density of states for the system $Ti_{1-x}Al_xN$ as a function of energy (in eV relative to the Fermi energy E_F) and fraction of AlN, x. In the case of pure TiN one can clearly see the peaks corresponding to the bonding (-8 to -3 eV) and nonbonding (-2 to 2 eV) states separated by a pseudogap. The N $2s$ states at about -15 eV are clearly separated from the rest of the valence band and play no significant role in the bonding for this system. Since the bonding states can only accommodate six valence electrons and there are a total of seven present (4 Ti+3 N) in the unit cell (not counting N-$2s$) one electron has to occupy the nonbonding states and the Fermi level is shifted above the minimum of the pseudogap.

In the case of pure c-AlN, the semiconducting character is clearly visible. The calculated band gap is 3.42 eV. We are not aware of an experimental value. When gradually increasing the Al content in $Ti_{1-x}Al_xN$ one can see that up to x

$=0.50$ there is a gradual, smooth change in the DOS. However, for the composition $x=0.75$ one can see that the DOS shows clear similarities with the one for pure AlN, but with an isolated Ti state within the band gap. This result can be explained by the fact that substitution of Ti by Al is destroying the hybridization between next-nearest-neighbor metal atoms, as there are no Al d states which could participate in the bonding. This localizes the nonbonding Ti d states in the band gap of the material with predominantly ionic bonds. Since Ti has one valence electron more than can be accommodated by the AlN valence band, the impurity state at E_F becomes populated.

In Fig. 8 the Ti-site projected DOS at E_f (in states per eV) is plotted as a function of a fraction of AlN. It is obvious that above $x=0.50$ the decrease of Ti-Ti hybridization leads to a dramatic increase of the local DOS at the Fermi level at the Ti sites. The destabilizing effect of a high DOS at the Fermi level is well known[14] and we suggest that the increase of Ti-site projected DOS at E_F is an indication of increased tendency towards decomposition in the $Ti_{1-x}Al_xN$ system.

The above effect also has a local environment aspect, as is illustrated in Fig. 9. Figure 9 shows the Ti-site projected density of states (PDOS) (in states per eV and unit cell) calculated for the supercell with $x=0.50$. The PDOS at two different Ti-atoms with different local environments are shown together with the Ti PDOS in pure TiN. One of the Ti atoms has next-nearest-neighbors consisting of 3 Al atoms and 9 Ti atoms (thick solid line) while the other atom has 9 Al and 3 Ti atoms (dashed line). There are clear differences, in particular the increase of the PDOS at E_F for the Ti atom in the Al-rich environment.

Thus, we suggest that the electronic structure effects described above are responsible for both the high mixing enthalpy as such and its strongly asymmetric concentration dependence, cf. Fig. 4.

E. Thermodynamical properties of c-$Ti_{1-x}Al_xN$

Using the EMTO method we have calculated the total energy with composition intervals of 5% as seen in Fig. 4. This gives a fine mesh in terms of alloy concentration that makes it possible to calculate accurately the second derivative of the mixing enthalpy with respect to the fraction of AlN. This is important in order to obtain information on alloy concentrations that show spinodal decomposition.

In order to avoid numerical noise in the evaluation of the second concentration derivative, Eq. (1), the fifth-order polynomial fit to $H(x)$ was used in in the derivation. A convergence test with respect to polynomial order was performed and the fifth order of the polynomial fit was found to give an accurate description of the second concentration derivative. However, if a polynomial fit with lower order is used, as is the case in Ref. 13, some important structure of the second derivative is lost. In Fig. 10 the mixing enthalpy and its second concentration derivative is shown together with the enthalpy of four different ordered $Ti_{0.5}Al_{0.5}N$ compounds.

The mixing enthalpy of $Ti_{1-x}Al_xN$ is found to be positive for all values of x. The curve is not symmetric, but has its highest value, 0.12 eV/atom, at about $x=0.68$. This shows

that the energy needed to solve a small amount of AlN in TiN is smaller than the energy required to solve an equal amount of TiN in c-AlN. This is a clear manifestation of the complex evolution of the electronic structure as discussed in the previous section.

$d^2H(x)/dx^2$ has a strong concentration dependence. It is only for low AlN content, with $x < 0.15$, that the spinodal condition is not fullfilled at 0 K. At large x the second derivative goes to very large numbers. This is a consequence of the nonsymmetric shape of the mixing enthalpy curve which at 0 K is the same as the free energy and indicates an extreme instability towards decomposition at high fractions of AlN. The plateau of $d^2H(x)/dx^2$ at intermediate concentrations on the other hand indicates that there might be a quite limited temperature intervall where a large part of the concentration range is moved out of the spinodal regime.

The four-ordered Ti$_{0.5}$Al$_{0.5}$N compounds shown in Fig. 10 are the $B1$ counterparts to the fcc-based structures $L10$, $L11$, double layer $L10$, and double layer $L11$. $L10$ consist of a fcc lattice where 001 planes are alternativly occupied by the two alloy components. $L11$ is similar but with the alternating planes stacked in the 111 direction. The double layered $L10$ is the structure shown in Fig. 2 while the double layered $L11$ has 111 planes of the same alloy component in the sequence A-A-B-B. In our $B1$ case it means that the metal sublattice is ordered acording to the corresponding fcc based structure while the nitrogen sublattice is kept homogenous. The large dispersion in mixing enthalpy of these different ordered compounds, despite the fact that they have the same composition and underlaying lattice, shows that there are strong local interactions in the system. This shows the importance of treating the substitutional disordered solid solution in a correct way if the random state is to be calculated. We underline that there exists ordered compounds that, even though they have positive mixing enthalpy, are considerably below the disordered phase in total energy. Their existence are likely to effect the decomposition thermodynamics and/or kinetics of the system.

In order to simulate the effect of increasing temperature we estimate the free energy per formula unit

$$G(x,T) = H(x) - TS(x) \qquad (9)$$

where $H(x)$ is the mixing enthalpy per formula unit. Within the mean-field approximation for the entropy

$$S_{mf}(x) = - k_B[x \ln(x) + (1-x)\ln(1-x)], \qquad (10)$$

where x is the fraction of AlN. This is so because in our case the mixing takes place only on one of the two sublattices and that the contribution to the entropy from the ordered-nitrogen sublattice is equal to zero. This aspect seems to have been overlooked in several previous publications on similar quasibinary systems.[10,13] The use of common tangent analysis of the free energy curves and the sign of the second concentration derivatives of the free energy allows us to estimate the phase diagram which is shown in Fig. 11.

This formula is a drastic simplification of the real entropy and is used only to obtain a guideline for further experiments or more realistic theoretical calculations. Especially in a system with strong local interactions such as the one in the present study we expect the mean-field approximation to give an overestimation of transition temperatures. Indeed short-range order lowers the free energy for the solid solution phase. The later is neglected by the mean-field approach.

Vibrational entropy is also neglected but this simplification is believed to be of less importance than the configurational one since the differnce in lattice parameter is so small.

The mean-field phase diagram suggests that c-Ti$_{1-x}$Al$_x$N should be subject to spinodal decomposition over a large range of the concentrations. At temperatures around 1000 K, often used in annealing experiments the spinodal region goes from about $x = 0.20$ to $x = 0.99$. Even though the phenomena of age hardening have been experimentally reported only for AlN fractions higher than 50%, there are signs of isostructural decomposition in experiments with AlN content as low as 40% and even 25%.[59–61]

Our results differ significantly from the mean-field phase diagram in Ref. 13. We attribute the major part of this difference to the fact that in Ref. 13 the entropy contribution was originally overestimated leading to a corresponding underestimation of transition temperatures.[62] However, our mixing enthalpies also are different and we believe that this is because of an inconsistent treatment of substitutional disorder in Ref. 13, where a couple of random number generated supercells with uncontrolled distribution of atoms was used. A subsequent least square fit to energies generated for these supercells was used for the estimate of the mixing enthalpy of the solid solution phase. The latter procedure would probably work if the size of the supercells is quite big to accomodate (average out) unavoidable fluctuations. However, it is not the case of Ref. 13. Anyway, the conclusion is possible to make only if the correlation functions of the supercells defined in Ref. 13 are known. On the other hand we have an entirely consistent results of two methods (supercells and CPA), which proves the reliability of our simulations.

IV. CONCLUSIONS

We have shown that the EMTO method in combination with the CPA and the independent sublattice model for the treatment of local lattice relaxations can be used to calculate mixing enthalpy of disordered $B1$ structure nitrides even if the effects of local lattice relaxations are large. The results are consistent with calculations within a supercell scheme. The accuracy and efficiency of this method makes it possible to perform total energy calculations with very small concentration intervals. This allows us to calculate the second concentration derivative of the mixing enthalpy with high accuracy.

We have used our method to calculate lattice parameters, electronic structure, mixing enthalpy, and the mean-field phase diagram of the $B1$ cubic Ti$_{1-x}$Al$_x$N system. The system is predicted to be within the unstable, spinodal regime over a large composition range at all relevant temperatures. However due to the strong local interactions in the system, manifested in large spread of the enthalpy of different ordered compounds with the same composition, we believe that the mean-field estimate strongly overestimates the phase separation temperatures. The strong asymmetry of both the mixing

enthalpy itself and its second concentration derivative are shown to be due to electronic structure effects. The main feature is the formation of a nonbonding atomiclike Ti d state at the Fermi level in a band gap of an Al-rich $Ti_{1-x}Al_xN$ alloy due to the absence of d-d next-nearest-neighbor hybridization between Ti and Al atoms. Our method opens the possibility to constructe reliable phase diagrams of $B1$ structure materials if methods that goes beyond the mean-field approximation is used for the entropy contribution. Also more complex multicomponent nitrides such as (Ti-Cr-Al)N, (Ti-Al-Y)N, and (Ti-Al-Si)N can be studied. Such work is currently in progress.

APPENDIX: SUPERCELL STRUCTURES AND SHORT-RANGE ORDER PARAMETERS

The distribution of Ti, Al, and N atoms in the supercells that have been used to simulate the random distribution of atoms for concentrations of $x=0.125$, $x=0.25$, $x=0.375$, $x=0.50$, $x=0.625$, $x=0.75$, and $x=0.875$ are given in Tables I–IV. The same supercells are used for x symmetric with respect to equiatomic compositions (e.g., $x=0.25$ and $x=0.75$). The only difference is that the Ti and Al atoms have been interchanged. This gives four distinct supercells. Note

TABLE I. Primitive translation vectors and atomic coordinates for the supercell used to calculate the total energy for the fractions of AlN $x=0.125$ and $x=0.875$ in $Ti_{1-x}Al_xN$ alloys.

Type	x	y	z	Type	x	y	z
P_1	0.500	0.500	0.000				
P_2	0.000	0.500	0.500				
P_3	0.250	0.000	0.250				
Al(Ti)	0.125	0.375	0.500	N	0.125	0.125	0.125
Al(Ti)	0.125	0.500	0.375	N	0.250	0.125	0.250
Al(Ti)	0.375	0.250	0.125	N	0.125	0.250	0.250
Al(Ti)	0.500	0.375	0.125	N	0.250	0.250	0.375
Ti(Al)	0.000	0.000	0.000	N	0.125	0.375	0.375
Ti(Al)	0.125	0.000	0.125	N	0.250	0.375	0.500
Ti(Al)	0.000	0.125	0.125	N	0.125	0.500	0.500
Ti(Al)	0.125	0.125	0.250	N	0.250	0.500	0.625
Ti(Al)	0.000	0.250	0.250	N	0.250	0.250	0.125
Ti(Al)	0.125	0.250	0.375	N	0.375	0.250	0.250
Ti(Al)	0.000	0.375	0.375	N	0.250	0.375	0.250
Ti(Al)	0.125	0.125	0.000	N	0.375	0.375	0.375
Ti(Al)	0.250	0.125	0.125	N	0.250	0.500	0.375
Ti(Al)	0.125	0.250	0.125	N	0.375	0.500	0.500
Ti(Al)	0.250	0.250	0.250	N	0.250	0.625	0.500
Ti(Al)	0.125	0.375	0.250	N	0.375	0.625	0.625
Ti(Al)	0.250	0.375	0.375	N	0.375	0.375	0.125
Ti(Al)	0.250	0.500	0.500	N	0.500	0.375	0.250
Ti(Al)	0.250	0.250	0.000	N	0.375	0.500	0.250
Ti(Al)	0.250	0.375	0.125	N	0.500	0.500	0.375
Ti(Al)	0.375	0.375	0.250	N	0.375	0.625	0.375
Ti(Al)	0.250	0.500	0.250	N	0.500	0.625	0.500
Ti(Al)	0.375	0.500	0.375	N	0.375	0.750	0.500
Ti(Al)	0.250	0.625	0.375	N	0.500	0.750	0.625
Ti(Al)	0.375	0.625	0.500	N	0.500	0.500	0.125
Ti(Al)	0.375	0.375	0.000	N	0.625	0.500	0.250
Ti(Al)	0.375	0.500	0.125	N	0.500	0.625	0.250
Ti(Al)	0.500	0.500	0.250	N	0.625	0.625	0.375
Ti(Al)	0.375	0.625	0.250	N	0.500	0.750	0.375
Ti(Al)	0.500	0.625	0.375	N	0.625	0.750	0.500
Ti(Al)	0.375	0.750	0.375	N	0.500	0.875	0.500
Ti(Al)	0.500	0.750	0.500	N	0.625	0.875	0.625

TABLE II. Primitive translation vectors and atomic coordinates for the supercell used to calculate the total energy for the fractions of AlN $x=0.25$ and $x=0.75$ in $Ti_{1-x}Al_xN$ alloys.

Type	x	y	z	Type	x	y	z
P_1	0.500	0.500	0.000				
P_2	0.000	0.375	0.375				
P_3	0.250	0.000	0.250				
Ti(Al)	0.000	0.000	0.000	N	0.125	0.125	0.125
Ti(Al)	0.125	0.000	0.125	N	0.250	0.125	0.250
Ti(Al)	0.000	0.250	0.250	N	0.125	0.250	0.250
Ti(Al)	0.125	0.250	0.375	N	0.250	0.250	0.375
Ti(Al)	0.125	0.125	0.000	N	0.125	0.375	0.375
Ti(Al)	0.250	0.125	0.125	N	0.250	0.375	0.500
Ti(Al)	0.125	0.250	0.125	N	0.250	0.250	0.125
Ti(Al)	0.125	0.375	0.250	N	0.375	0.250	0.250
Ti(Al)	0.250	0.375	0.375	N	0.250	0.375	0.250
Ti(Al)	0.250	0.250	0.000	N	0.375	0.375	0.375
Ti(Al)	0.375	0.250	0.125	N	0.250	0.500	0.375
Ti(Al)	0.250	0.375	0.125	N	0.375	0.500	0.500
Ti(Al)	0.375	0.375	0.250	N	0.375	0.375	0.125
Ti(Al)	0.250	0.500	0.250	N	0.500	0.375	0.250
Ti(Al)	0.375	0.500	0.375	N	0.375	0.500	0.250
Ti(Al)	0.375	0.500	0.125	N	0.500	0.500	0.375
Ti(Al)	0.500	0.500	0.250	N	0.375	0.625	0.375
Ti(Al)	0.500	0.625	0.375	N	0.500	0.625	0.500
Al(Ti)	0.000	0.125	0.125	N	0.500	0.500	0.125
Al(Ti)	0.125	0.125	0.250	N	0.625	0.500	0.250
Al(Ti)	0.250	0.250	0.250	N	0.500	0.625	0.250
Al(Ti)	0.375	0.375	0.000	N	0.625	0.625	0.375
Al(Ti)	0.500	0.375	0.125	N	0.500	0.750	0.375
Al(Ti)	0.375	0.625	0.250	N	0.625	0.750	0.500

that all the coordinates for technical reasons are scaled with a factor 0.25 compared to the case where the side of the conventional unit cell is set to 1 in units of the lattice parameter. In Table V the short-range order parameters for the different supercells are given.

TABLE III. Primitive translation vectors and atomic coordinates for the supercell used to calculate the total energy for the fractions of AlN $x=0.375$ and $x=0.625$ in $Ti_{1-x}Al_xN$ alloys.

Type	x	y	z	Type	x	y	z
P_1	0.500	0.500	0.000				
P_2	0.000	0.500	0.500				
P_3	0.250	0.000	0.250				
Al(Ti)	0.125	0.000	0.125	N	0.125	0.125	0.125
Al(Ti)	0.000	0.375	0.375	N	0.250	0.125	0.250
Al(Ti)	0.125	0.375	0.500	N	0.125	0.250	0.250
Al(Ti)	0.125	0.125	0.000	N	0.250	0.250	0.375
Al(Ti)	0.250	0.250	0.250	N	0.125	0.375	0.375
Al(Ti)	0.125	0.375	0.250	N	0.250	0.375	0.500
Al(Ti)	0.250	0.500	0.500	N	0.125	0.500	0.500
Al(Ti)	0.250	0.250	0.000	N	0.250	0.500	0.625
Al(Ti)	0.375	0.250	0.125	N	0.250	0.250	0.125
Al(Ti)	0.375	0.625	0.500	N	0.375	0.250	0.250
Al(Ti)	0.500	0.625	0.375	N	0.250	0.375	0.250
Al(Ti)	0.375	0.750	0.375	N	0.375	0.375	0.375
Ti(Al)	0.000	0.000	0.000	N	0.250	0.500	0.375
Ti(Al)	0.000	0.125	0.125	N	0.375	0.500	0.500
Ti(Al)	0.125	0.125	0.250	N	0.250	0.625	0.500
Ti(Al)	0.000	0.250	0.250	N	0.375	0.625	0.625
Ti(Al)	0.125	0.250	0.375	N	0.375	0.375	0.125
Ti(Al)	0.250	0.125	0.125	N	0.500	0.375	0.250
Ti(Al)	0.125	0.250	0.125	N	0.375	0.500	0.250
Ti(Al)	0.250	0.375	0.375	N	0.500	0.500	0.375
Ti(Al)	0.125	0.500	0.375	N	0.375	0.625	0.375
Ti(Al)	0.250	0.375	0.125	N	0.500	0.625	0.500
Ti(Al)	0.375	0.375	0.250	N	0.375	0.750	0.500
Ti(Al)	0.250	0.500	0.250	N	0.500	0.750	0.625
Ti(Al)	0.375	0.500	0.375	N	0.500	0.500	0.125
Ti(Al)	0.250	0.625	0.375	N	0.625	0.500	0.250
Ti(Al)	0.375	0.375	0.000	N	0.500	0.625	0.250
Ti(Al)	0.500	0.375	0.125	N	0.625	0.625	0.375
Ti(Al)	0.375	0.500	0.125	N	0.500	0.750	0.375
Ti(Al)	0.500	0.500	0.250	N	0.625	0.750	0.500
Ti(Al)	0.375	0.625	0.250	N	0.500	0.875	0.500
Ti(Al)	0.500	0.750	0.500	N	0.625	0.875	0.625

TABLE IV. Primitive translation vectors and atomic coordinates for the supercell used to calculate the total energy for the fraction of AlN $x=0.50$ in $Ti_{1-x}Al_xN$ alloy.

Type	x	y	z	Type	x	y	z
P_1	0.500	0.500	0.000				
P_2	0.000	0.375	0.375				
P_3	0.250	0.000	0.250				
Ti	0.125	0.000	0.125	N	0.125	0.125	0.125
Ti	0.125	0.125	0.250	N	0.250	0.125	0.250
Ti	0.000	0.250	0.250	N	0.125	0.250	0.250
Ti	0.125	0.125	0.000	N	0.250	0.250	0.375
Ti	0.250	0.250	0.000	N	0.125	0.375	0.375
Ti	0.375	0.375	0.250	N	0.250	0.375	0.500
Ti	0.250	0.500	0.250	N	0.250	0.250	0.125
Ti	0.500	0.375	0.125	N	0.375	0.250	0.250
Ti	0.375	0.500	0.125	N	0.250	0.375	0.250
Ti	0.500	0.500	0.250	N	0.375	0.375	0.375
Ti	0.375	0.625	0.250	N	0.250	0.500	0.375
Ti	0.500	0.625	0.375	N	0.375	0.500	0.500
Al	0.000	0.000	0.000	N	0.375	0.375	0.125
Al	0.000	0.125	0.125	N	0.500	0.375	0.250
Al	0.125	0.250	0.375	N	0.375	0.500	0.250
Al	0.250	0.125	0.125	N	0.500	0.500	0.375
Al	0.125	0.250	0.125	N	0.375	0.625	0.375
Al	0.250	0.250	0.250	N	0.500	0.625	0.500
Al	0.125	0.375	0.250	N	0.500	0.500	0.125
Al	0.250	0.375	0.375	N	0.625	0.500	0.250
Al	0.375	0.250	0.125	N	0.500	0.625	0.250
Al	0.250	0.375	0.125	N	0.625	0.625	0.375
Al	0.375	0.500	0.375	N	0.500	0.750	0.375
Al	0.375	0.375	0.000	N	0.625	0.750	0.500

TABLE V. Short-range order (SRO) parameters for the supercells used to model the different fractions of AlN in the $Ti_{1-x}Al_xN$ alloy. The SRO parameters are given for the *metallic* coordination shells.

	Shell						
Fraction AlN	1	2	3	4	5	6	7
0.125, 0.875	0.00	−0.04	−0.04	0.04	0.00	0.14	−0.04
0.25, 0.75	0.00	−0.03	−0.03	0.00	0.00	0.05	−0.04
0.375, 0.625	0.00	−0.02	−0.02	0.02	0.00	0.06	−0.02
0.50	0.00	0.00	0.00	0.00	−0.05	0.00	0.00

*Electronic address: bjoal@ifm.liu.se

[1] R. Lamni, R. Sanjines, M. Parlinska-Wojtan, A. Karimi, and F. Levy, J. Vac. Sci. Technol. A **23**, 593 (2005).

[2] M. Parlinska-Wojtan, A. Karimi, O. Coddet, T. Cselle, and M. Morstein, Surf. Coat. Technol. **188**, 344 (2004).

[3] I. Grimberg, V. N. Zhitormirsky, R. L. Boxman, S. Goldsmith, and B. Z. Weiss, Surf. Coat. Technol. **108**, 154 (1998).

[4] A. Zaoui, B. Bouhafs, and P. Ruterana, Mater. Chem. Phys. **91**, 108 (2005).

[5] A. Hörling, L. Hultman, M. O. J. Sjölén, and L. Karlsson, Surf. Coat. Technol. **191**, 384 (2005).

[6] P. H. Mayrhofer, A. Hörling, L. Karlsson, J. Sjölén, T. Larsson, C. Mitterer, and L. Hultman, Appl. Phys. Lett. **83**, 2049 (2003).

[7] D. Gall, S. Kodambaka, M. A. Wall, I. Petrov, and J. E. Greene, J. Appl. Phys. **93**, 9086 (2003).

[8] H. Hugosson, H. Högberg, M. Algren, M. Rodmar, and T. I. Selinder, J. Appl. Phys. **93**, 4505 (2003).

[9] L. K. Teles, L. M. R. Scolfaro, J. R. Leite, J. Furthmüller, and F. Bechstedt, Appl. Phys. Lett. **80**, 1177 (2001).

[10] M. Ferhat and F. Bechstedt, Phys. Rev. B **65**, 075213 (2002).

[11] L. K. Teles, J. Furthmüller, L. M. R. Scolfaro, J. R. Leite, and F. Bechstedt, Phys. Rev. B **62**, 2475 (2000).

[12] S. Y. Karpov, N. I. Podolskaya, I. A. Zhmakin, and A. I. Zhmakin, Phys. Rev. B **70**, 235203 (2004).

[13] P. H. Mayrhofer, D. Music, and J. M. Schneider, Appl. Phys. Lett. **88**, 071922 (2006).

[14] E. A. Smirnova, P. A. Korzhavyi, Y. K. Vekilov, B. Johansson, and I. A. Abrikosov, Phys. Rev. B **64**, 020101 (2001); Eur. Phys. J. B **30**, 57 (2002).

[15] P. Olsson, I. A. Abrikosov, L. Vitos, and J. Wallenius, J. Nucl. Mater. **321**, 84 (2003); P. Olsson, I. A. Abrikosov, and J. Wallenius, Phys. Rev. B **73**, 104416 (2006).

[16] A. V. Ruban, S. I. Simak, S. Shallcross, and H. L. Skriver, Phys. Rev. B **67**, 214302 (2003).

[17] A. E. Kissavos, S. Shallcross, V. Meded, L. Kaufman, and I. A. Abrikosov, CALPHAD: Comput. Coupling Phase Diagrams Thermochem. **29**, 17 (2005).

[18] L. Vitos, H. L. Skriver, B. Johansson, and J. Kollár, Comput. Mater. Sci. **18**, 24 (2000).

[19] L. Vitos, Phys. Rev. B **64**, 014107 (2001).

[20] L. Vitos, Recent Res. Dev. Phys. **5**, 103 (2004).

[21] O. K. Andersen, O. Jepsen, and G. Krier, in *Lecture on Methods of Electronic Structure Calculations*, edited by V. Kumar, O. K. Andersen, and A. Mookerjee (World Scientific, Singapore, 1994), p. 63.

[22] O. K. Andersen, C. Arcangeli, R. W. Tank, T. Saha-Dasgupta, G. Krier, O. Jepsen, and I. Dasgupta, in *Third-Generation TB-LMTO*, MRS Symposia Proceedings No. 491 (Materials Research Socity, Pittsburgh, 1998), p. 3.

[23] O. K. Andersen, T. Saha-Dasgupta, R. W. Tank, C. Arcangeli, O. Jepsen, and G. Krier, in *Electronic Structure and Physical Properties of Solids: The Uses of the LMTO Method*, edited by H. Dreysseé, Lectures Notes in Physics Vol. 535 (Springer-Verlag, Berlin, 2000), pp. 3–84.

[24] O. K. Andersen and T. Saha-Dasgupta, Phys. Rev. B **62**, R16219 (2000).

[25] L. Vitos, J. Kollár, and H. L. Skriver, Phys. Rev. B **55**, 13521 (1997).

[26] J. Kollár, L. Vitos, and H. L. Skriver, in *Electronic Structure and Physical Properties of Solids: The Uses of the LMTO Method*, Ref. [23], pp. 85–113.

[27] J. Kollár, L. Vitos, J. M. Osorio-Guillén, and R. Ahuja, Phys. Rev. B **68**, 245417 (2003).

[28] L. Chioncel, L. Vitos, I. A. Abrikosov, J. Kollár, M. I. Katsnelson, and A. I. Lichtenstein, Phys. Rev. B **67**, 235106 (2003).

[29] B. Magyari-Köpe, L. Vitos, G. Grimvall, B. Johansson, and J. Kollár, Phys. Rev. B **65**, 193107 (2002).

[30] L. Vitos, I. A. Abrikosov, and B. Johansson, Phys. Rev. Lett. **87**, 156401 (2001).

[31] B. Magyari-Köpe, G. Grimvall, and L. Vitos, Phys. Rev. B **66**, 064210 (2002).

[32] L. Vitos, P. A. Korzhavyi, and B. Johansson, Phys. Rev. Lett. **88**, 155501 (2002).

[33] L. Vitos, P. A. Korzhavyi, and B. Johansson, Nat. Mater. **2**, 25 (2003).

[34] L. Dubrovinsky *et al.*, Nature (London) **422**, 58 (2003).

[35] A. V. Ruban, S. Shallcross, S. I. Simak, and H. L. Skriver, Phys. Rev. B **70**, 125115 (2004).

[36] J. W. Morgan, J. Phys. C **10**, 1181 (1976).

[37] J. P. Perdew, K. Burke, and M. Ernzerhof, Phys. Rev. Lett. **77**, 3865 (1996).

[38] I. A. Abrikosov, A. M. N. Niklasson, S. I. Simak, B. Johansson, A. V. Ruban, and H. L. Skriver, Phys. Rev. Lett. **76**, 4203 (1996).

[39] I. A. Abrikosov, S. I. Simak, B. Johansson, A. V. Ruban, and H. L. Skriver, Phys. Rev. B **56**, 9319 (1997).

[40] P. E. Blöchl, Phys. Rev. B **50**, 17953 (1994).

[41] G. Kresse and J. Hafner, Phys. Rev. B **48**, 13115 (1993).

[42] G. Kresse and J. Hafner, Phys. Rev. B **49**, 14251 (1994).

[43] By a distinct cluster one understands a pair of nearest-neighbor atoms, a pair of next-nearest-neighbor atoms, a triangle between three atoms, etc.

[44] J. M. Sanchez, F. Ducastelle, and D. Gratias, Physica A **128**, 334 (1984).

[45] F. Ducastelle, *Order and Phase Stability in Alloys* (North-Holland, Amsterdam, 1991).

[46] A. Zunger, S. H. Wei, L. G. Ferreira, and J. E. Bernard, Phys. Rev. Lett. **65**, 353 (1990).

[47] S. H. Wei, L. G. Ferreira, J. E. Bernard, and A. Zunger, Phys. Rev. B **42**, 9622 (1990).

[48] Picture taken from the Crystal Lattice Structures Web page, http://cst-www.nrl.navy.mil/lattice/, provided by the Center for Computational Materials Science of the United States Naval Research Laboratory.

[49] F. Adibi, I. Petrov, J. Greene, U. Wahlström, and J.-E. Sundgren, J. Vac. Sci. Technol. A **11**, 136 (1993).

[50] U. Wahlström, L. Hultman, J.-E. Sundgren, F. Adibi, I. Petrov, and J. E. Greene, Thin Solid Films **235**, 62 (1993).

[51] Powder Diffraction File *c*-AlN: [25-1495] TiN:, [6-642], JCPDC International Center for Powder Diffraction Data, Swarthmore, PA, 1994.

[52] H. Vollstädt, E. Ito, M. Akaishi, S. Akimoto, and O. Fukunaga, Proc. Jpn. Acad., Ser. B: Phys. Biol. Sci. **66**, 7 (1990).

[53] C. Stampfl, W. Mannstadt, R. Asahi, and A. J. Freeman, Phys. Rev. B **63**, 155106 (2001).

[54] C. D. Gelatt, A. R. Williams, and V. L. Moruzzi, Phys. Rev. B **27**, 2005 (1983).

[55] D. L. Price and B. R. Cooper, Phys. Rev. B **39**, 4945 (1989).

[56] J. Häglund, A. Fernández Guillermet, G. Grimvall, and M. Körling, Phys. Rev. B **48**, 11685 (1993).

[57] S. H. Jhi and J. Ihm, Phys. Rev. B **56**, 13826 (1997).

[58] P. E. Van Camp, V. E. Van Doren, and J. T. Devreese, Phys. Rev. B **44**, 9056 (1991).

[59] A. E. Santana, A. Karimi, V. H. Derflinger, and A. Schutze, Tribol. Lett. **17**, 689 (2004).

[60] A. Hörling, L. Hultman, M. Oden, J. Sjölén, and L. Karlsson, J.

Vac. Sci. Technol. A **20**, 1815 (2002).

[61] A. Hörling, Ph.D. thesis, Linköping Studies in Science and Technology, 2005.

[62] P. H. Mayrhofer, D. Music, and J. M. Schneider, Appl. Phys. Lett. (to be published), erratum to Ref. 13.